PERFORMANCE INVESTIGATION OF INNOVATIVE COMPACT POROUS CERAMIC HEAT EXCHANGER

***Abstract*: Designing efficient and compact heat exchangers is essential to enhance energy utilization and improve the overall performance of energy systems. In this study, the performance of an innovative compact porous ceramic heat exchanger configuration is examined. A numerical model based on Whitaker theory is developed to accurately evaluate heat and mass transfer within an unsaturated porous ceramic exchanger. To simulate the transport phenomena occurring during convective exchange, a three-dimensional unstructured Control Volume Finite Element Method (CVFEM) is implemented. Several numerical investigations are performed to assess the influence of porosity, hot air velocity, and the initial saturation of the ceramic medium. The temporal evolution of temperature, liquid saturation, and pressure within the porous domain is analyzed and compared. The heat exchange rate increases as the initial liquid saturation of the porous ceramic medium decreases, while the mass transfer efficiency improves with higher air velocity. Moreover, the porosity of the ceramic material plays a crucial role in maximizing heat exchange. The results show that doubling the air velocity reduces the exchange time by half compared to the reference case with a hot air velocity of V = 5 m/s.**

***Keywords:* heat exchangers, porous ceramic, CVFEM, ceramic medium**

Nomenclature

C_a	specific heat of the air $[kJ/kgK]$	Greek letters	
C_p	specific heat at constant pressure $[kJ/kgK]$	ε	porosity
C_v	specific heat of the vapor $[kJ/kgK]$	ε_l	volume fraction of liquid phase
C_w	specific heat of the water $[kJ/kgK]$	μ	dynamic viscosity [kg/ms]
$D_{A,B}$	Diffusion coefficient [m^2/s]	ϑ	kinematic viscosity $[m^2/s]$
g	gravitational acceleration [m/s^2]	ρ	density [kg/m^3]
h_m	convective mass transfer	λ	conductive transfer coefficient

	coefficient[m/s]		[$W/m°C$]
h_t	convective heat transfer coefficient[$W/m^2°C$]	σ	surface tension [N/m]
K	intrinsic permeability [m²]	ΔH_{vap}	vaporisation latent heat [J / Kg]
L_c	characteristic length of brick [m]		
M	molar mass of air [kg/mol]	Subscripts	
		0	initial condition
ṁ	evaporation rate [kg/s]	a	air
n_i	outward normal vector	eff	effective
P	pressure [Pa]	g	Gas
Pc	capillary pressure [Pa]	l	liquid
Po	Exchanger porosity [%]	v	vapor
P_{Vs}	partial pressure of saturated vapour [Pa]	vs	Saturated vapor

1. INTRODUCTION

Heat transmission has recently been the subject of numerous studies. Heat transfer is found in many conversion systems and devices that involve the use of heat exchangers. As a result, porous media, which significantly improve heat and mass transport, have seen a variety of industrial applications. It's worth noting that more study on porous media's potential, especially on heat exchangers, is necessary. In this study, the focus will be on examining heat and mass transfer within unsaturated porous ceramic exchangers.

The development of a numerical model was presented and described. This model predicts heat and mass transport based on the Whitaker theory, it uses a three-dimensional unstructured Control Volume Finite Element Method to evaluate the convective exchange process with various operating parameters, aiming at a parametric study for achieving optimal thermal performance and overall efficiency for the compact heat exchanger under consideration [1]. Intrinsic permeability and inertial coefficients are taken into account, respectively determined by empirical correlations related to the porous core's geometric characteristics [2]. According to the numerical experiments, heat transfer rates and the average outlet fluid temperature were improved when porosity was decreased for several mass flow rates [3]. Optimization potential can be achieved in terms of pore morphology and materials, and structure design for new more mechanically robust and longer lasting structure [4].

Characterization of the porous structure is important to understand the implications of any changes that are made to their performance and to help in an efficient design. In fact, the minimization of thermal resistances, during the design of compact heat exchangers, leads to

an improvement of heat transfer and a reduction of thermal dissipation [5]. An open-cell foams' multiscale model was established and studied to cover different materials, cell sizes, and porosities for a proper characterization of the heat exchanger [6]. In the model, it was possible to obtain a complete description of the porous material by a set of main properties of porous media, such as pressure loss coefficients, heat conductivity, and Nusselt numbers in porous media, especially in anisotropic media [7]. This data can be used as input for a macroscopic model in order to predict the global performance of the entire device.

The important detail is that, in this case, it is not the Roseland type of modeling (simple) but a multilayered model that characterizes the microstructure of porous ceramic foam and that can be an input for macroscopic modeling. In fact, the flow motion's complex effect on the heat transfer process occurring in porous media, over a spatial problem in the porous domain, requires a robust numerical method and an efficient meshing that can characterize the fluid-solid interface [8]. The porous medium's morphological characteristics (aspect of the pores like pore size distribution, connectivity) also have an impact on the effective thermal conductivity and the permeability and they directly affect the thermal-hydraulic performance of the exchanger [9].

The potential of materials with a high specific surface area has been tested for the design of high-performance heat transfer applications including compact heat exchangers [10]. The porous structure's geometry has a direct impact on thermal and fluid dynamic responses, and a multistage modeling approach can be introduced to optimize the advanced ceramic heat exchanger design [11-12].

Thermal conductivity as a design input parameter for a heat transfer device can affect its overall performance [13]. Macroscopic models with effective transport properties can be derived by direct pore-level numerical simulations of complex porous geometry [14-15]. Optimization of the design of the heat exchanger is needed because porous materials' complex anisotropic nature is a challenging task [16-14]. Recently, the optimization design and performance study of a heat exchanger for an oil and gas recovery system in an oil depot has ben developed [17]. Also, Geunhyeong et al. have studied the design optimization of heat exchanger using deep reinforcement learning [18].

In conclusion, this study is aiming at an investigation of the coupled heat and mass transfer in a porous compact ceramic exchanger using a 3-D numerical model. The model was based on Whitaker theory using the Control Volume Finite Method. The influence of porosity, hot air velocity, and initial ceramic saturation has been studied by variations of temperature, liquid saturation, and pressure during the considered time in the porous domain.

2. Problem statement and Formulation

The present problem is a numerical study of heat and mass transfer inside a porous ceramic heat exchanger. The schematic diagram of porous compact heat exchanger is shown in Fig. 1. The material of the Heat exchanger is of ceramic with the width, length and height of 8 cm, 10 cm and 8cm, respectively. The ceramic domain is supposed to be unsaturated porous material with porosity 0.7, 0.5, 0.3 and 0.1 respectively are considered in the current study.

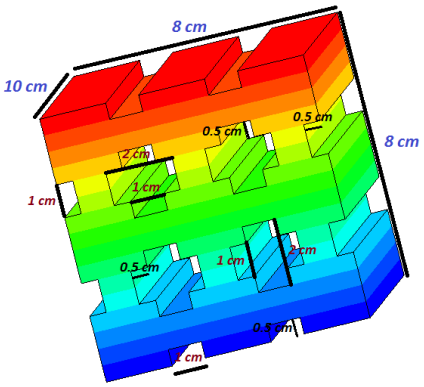

Fig. 1. Porous heat exchanger geometry.

2.1. Numerical equations

The system of equations is defined by a reference to Whitaker's theory [19]. A numerical model of heat and mass transfer is established for the unsaturated porous media and the following assumptions have place:

- We consider that the porous medium is homogenous and isotropic and the three phases (solid, liquid, gas) are in local thermodynamic equilibrium.
- We neglect the viscous dissipation, the compression-work and the radiative heat transfer.
- The gaseous phase is ideal (thermodynamic sense) and the dispersion and tortuosity terms are used as diffusion term.

In this context, the macroscopic equations of heat and mass transfer in porous media are:

- Generalized Darcy's Law:

Referring to Darcy's law, the average velocities (liquid phase ($\overline{V_l}$) and gaseous phase ($\overline{V_g}$)) are defined as bellow:

- *Liquid:*

$$\overline{V_l} = -\frac{KK_l}{\mu_l}\left[\nabla\left(\overline{P_g}^g - P_c\right) - \overline{\rho_l}^l g\right] \quad (1)$$

And $P_c = \overline{P_g}^g - \overline{P_l}^l$ presents the capillary pressure.

- *Gas (without applying the gravitational effect):*

$$\overline{V_g} = -\frac{KK_g}{\mu_g}\nabla\overline{P_g}^g \quad (2)$$

- Mass conservation:

- *Liquid:*

The equation of mass conservation for liquid phase is (liquid density is constant):

$$\frac{\partial \varepsilon_l}{\partial t} + \nabla(\overline{V_l}) = -\frac{\dot{m}}{\overline{\rho}_l} \quad (3)$$

With $\dot{m}$: the rate mass of the evaporation.

ε_l : the fraction volume of liquid

- *Gas:*

The equation of mass conservation for gaseous phase is:

$$\frac{d\overline{\rho_g}}{dt} + \nabla\left(\overline{\rho_g}^g \overline{V_g}\right) = \dot{m}_g \quad (4)$$

With $\overline{\rho}_g^g$: the average density intrinsic of gaseous phase. Also, this phase is considered as an ideal mixture of perfect gases.

- *Vapor:*

$$\frac{d\overline{\rho_v}}{dt} + \nabla\left(\overline{\rho_v}^g \overline{V_v}\right) = \dot{m}_v \quad (5)$$

$$\overline{\rho_v}^g \overline{V_v} = \overline{\rho_v}^g \overline{V_g} - \overline{\rho_g}^g D_{eff} \nabla\left(\frac{\overline{\rho_v}}{\overline{\rho_g}^g}\right) \quad (6)$$

D_{eff} presents the effective diffusion coefficient of vapor in porous medium. However, this coefficient takes into account the resistance to the diffusion due to the constriction and the tortuosity effects.

- Energy conservation:

The equation of energy conservation is defined as bellow:

$$\frac{\partial}{\partial t}(\overline{\rho C_P}\bar{T}) + div\left[\left(\bar{\rho_l}^{l} C_{Pl}\bar{V_l} + \sum_{k=a,V}\overline{\rho_k}^{g} C_{Pk}\overline{V_k}\right)\bar{T}\right] = \nabla\left(\lambda_{eff}.\nabla\bar{T}\right) - \Delta H_{vap}\ \dot{m}_v \quad (7)$$

With ΔH_{vap} : heat latent of vaporization at temperature T(K).

λ_{eff} : thermal effective conductivity of porous medium.

$\overline{\rho C_p}$: heat capacity of the porous medium defined as bellow:

$$\overline{\rho C_p} = \bar{\rho}_s C_{ps} + \bar{\rho}_l C_{pl} + \bar{\rho}_a C_{pa} + \bar{\rho}_v C_{pv} \quad (8)$$

Which $\bar{\rho}_s C_{ps}, \bar{\rho}_l C_{pl}$, $\bar{\rho}_v C_{pv}$ and $\bar{\rho}_a C_{pa}$ presents the mass heat capacities of three phases (solid, liquid, vapour and air).

- Thermodynamic relations:

The partial pressure of vapour is defined as bellow:

$P_v = P_{veq}(T, S)$.

With S: saturation of liquid explained by:

$$S = \frac{\varepsilon_l}{\varepsilon} \quad (9)$$

For the gaseous phase, the pressure is:

$$\bar{P}_i = \frac{\bar{\rho}_i}{M_i} R\bar{T} \ ;i=a,v \quad (10)$$

$$\bar{P}_g = \bar{P}_a + \bar{P}_v\ ,\ \bar{\rho}_g = \bar{\rho}_a + \bar{\rho}_v$$

For the vapor, the pressure is defined by:

$$\frac{Pv}{Pvs} = \exp\left(-\frac{2.\sigma.M_v}{r.\rho_l.R.T}\right) \quad (11)$$

2.2. Boundary and initial conditions

Initially, all fields; the temperature, saturation and pressure are uniform in the heat exchanger domain (Fig. 2).

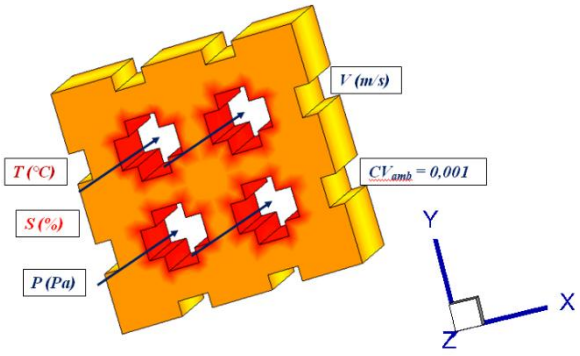

Fig. 2. Exchanger's boundary conditions.

The boundary conditions for our model are defined as following:

The exchanging cavities (highlighted in red in Fig.2):

$$\left[\lambda_{eff}\frac{\partial\langle T\rangle}{\partial X_i}+\Delta H_{vap}\rho_l\langle V_l\rangle n_i\right]=h_t\left(\langle T\rangle-T_\infty\right) \tag{12}$$

The mass flow (evacuation and evaporation):

$$\left[\rho_l\langle V_l\rangle+\langle\rho_v\rangle^g\langle V_v\rangle\right]n_i=h_m\left(C_{vs}-C_{v\infty}\right) \tag{13}$$

On exchanging cavities, the pressure is considered as the atmospheric pressure:

$$\left[\langle P_g\rangle^g\right]=P_{atm} \tag{14}$$

The external faces (right, left, up, bottom) are considered as adiabatic and impermeable faces.

$$\left[\lambda_{eff}\frac{\partial\langle T\rangle}{\partial X_i}+\Delta H_{vap}\rho_l\langle V_l\rangle n_i\right]=0 \tag{15}$$

$$\left[\rho_l\langle V_l\rangle+\langle\rho_v\rangle^g\langle V_v\rangle\right]n_i=0 \tag{16}$$

$$\left[\frac{\partial\langle P_g\rangle^g}{\partial X_i}\right]=0 \tag{17}$$

The convective coefficients (heat and mass transfer) are presented in Table 1.

Table 1. Convective coefficients for heat and mass transfer.

	Cavities [20]	**Faces [21]**
h_t	$\frac{\lambda\times 0.023\times \mathrm{Re}^{4/5}\times \mathrm{Pr}^{1/3}}{D}$	$\frac{\lambda\times 0.023\times \mathrm{Re}^{4/5}\times \mathrm{Pr}^{1/3}}{L_C}$
h_m	$\frac{D_{A,B}\times 0.023\times \mathrm{Re}^{4/5}\times \mathrm{Sc}^{1/3}}{D}$	$\frac{D_{A,B}\times 0.023\times \mathrm{Re}^{4/5}\times \mathrm{Sc}^{1/3}}{L_C}$
Validity	$10^4 < Re < 1.2\times 10^5$	$\mathrm{Re} < 5\times 10^5$

	$0.6 \leq Pr \leq 160$ $0.6 \leq Sc \leq 160$	$Pr \geq 0.6$ $Sc \geq 0.6$
Re	$\frac{\rho_a w_a D}{\mu_a}$	$\frac{\rho_a w_a L_C}{\mu_a}$
$Pr = \frac{C_a \mu_a}{\lambda_a}$		$Sc = \frac{\vartheta_a}{D_{A,B}}$

Which:

h_t : Convective coefficient of heat transfer $[{}^{W}/_{m^2 °C}]$

h_m: Convective coefficient of mass transfer $[{}^{m}/_{s}]$

$D_{A,B}$: Vapor diffusion in air defined as bellow:

$D_{A,B} = D_{vap\,,air} = 0.26 \times 10^{-4}\ [{}^{m^2}/_{s}]$

$L_C = 0.1$ m presents the characteristic length of the exchanger.

3. Numerical solution, grid dependency and validation

The Control Volume Finite Element Method (CVFEM) is used to solve our system of equations [22;23]. Moreover, the control volume is composed of prismatic elements which ensure the grid flexibility and the conservation of flux.

For the mesh generation, the free mesh generator Gmsh is employed (Fig. 3). The heat exchanger domain is divided in six-node prisms. Also, the centred of the triangular elements (prism's base) are joined to the midpoints of the corresponding sides.

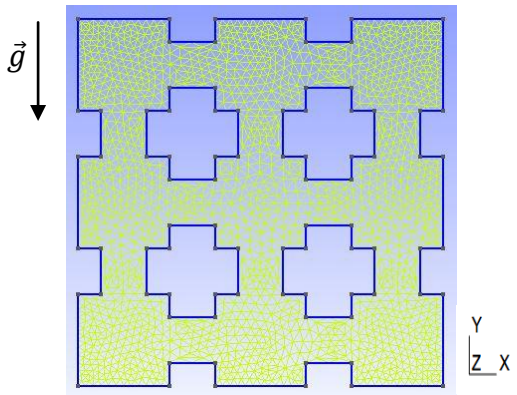

Fig. 3 Cross section of the 3D domain meshing.

- Grid dependency

Because of the relevance of grid size on the accuracy of numerical findings, grid independency tests were carefully performed. The initial and operating conditions are depicted in table 2. In Fig. 4, the equivalent liquid saturation and temperature of the porous media are compared for four grid sizes (Table 3) under the identical boundary conditions.

The mesh set (N = 35420) is chosen to carry out all of the simulations in this research in order to retain an acceptable degree of accuracy while minimizing computing costs as much as possible.

Table 2. Initial and operating conditions for the validation tests

Initial temperature	Initial saturation	Hot air temperature	Hot air velocity	porosity
20°C	50%	100°C	20m/s	0.1

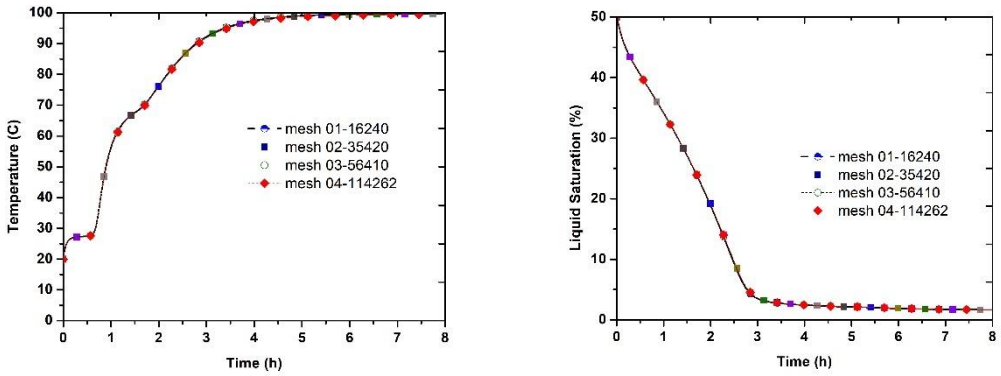

(A) ***(B)***

Fig. 4 Grid dependency of temperature (A) and liquid saturation (B).

Table 3. Grid dependency test

Cases	Case I	Case II	Case III	Case IV
Number of nodes	16240	35420	56410	114262

- Model validation

A numerical code (Fortran) has been developed to solve the coupled heat and mass transfer equations. The model is validated by the study of Hussain et al. [24]. Heat and mass transmission across porous tubular ceramic membranes were investigated experimentally by the authors (porous aluminum oxide). This research incorporates combined heat and mass transfer to provide insight into how temperature distribution and heat transmission across

porous membranes impact mass transport. Experiments were carried out in this work using tubular ceramic membranes with a length of L = 250 mm, an inner radius of $r_{m,i}$=10.5 mm and outer radius of $r_{m,o}$ =16 mm. The input flow velocity of the gas in the annulus varied from u_{in} = 0.44 m/s in these tests, with the imposed heat flux corresponding to a heat flow rate of of $\dot{Q}_i$=50 W. With the great agreement shown in Fig. 5, it can be concluded that the model developed to simulate mass and heat transport within porous exchangers is accurate and reliable enough to be used in this investigation.

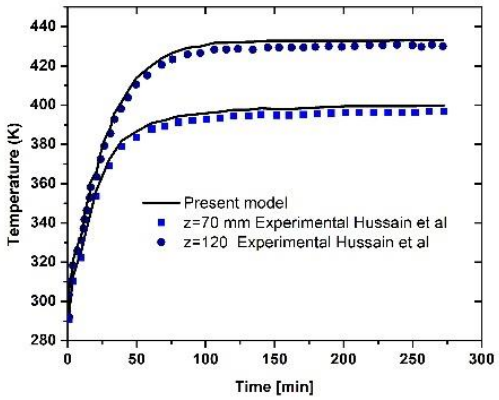

Fig.5 Evaluation of the current model's transient temperature results compared to those of Hussain et al. [24], at two different axial locations.

4. Results and discussions

In this section, we present the numerical results obtained for the simulation of heat and mass transfer within the considered compact porous exchanger.

The findings section is composed of three parts:

- Effect of hot exchanging air temperature.
- Effect of initial saturation of porous domain.
- Effect of porosity.
- Effect of hot air velocity.

4.1. Effect of hot exchanging air temperature

In this part, the effect of the hot exchanging air temperature has been evaluated. Therefore, four cases have been tested (Table 4).

Table 4. Operating and initial conditions for four studied cases

	T (°C)	**S_{in}** (%)	**T_{in}** (°C)	**V** (**m/s**)	**PO** -	**CV_{amb}**	**P_{amb}** (**atm**)
Case A	100	50	20	5	0.1	0.001	1
Case B	80	50	20	5	0.1	0.001	1
Case C	60	50	20	5	0.1	0.001	1
Case D	40	50	20	5	0.1	0.001	1

The three figures 6–8 present respectively the thermal, mass-transfer, and pressure responses of the unsaturated porous ceramic heat exchanger for different values of the hot exchanging-air temperature T. The temperatures T = 100, 80, 60 and 40 °C have been considered, which are the values considered in Cases A–D, respectively. The four cases have been processed under the same operating conditions, with same initial saturation, velocity, permeability and external pressure.

Fig. 6 shows that the time evolution of the averaged porous domain temperature is highly affected by the hot air temperature and the initial saturation. Since the ceramic is considered as unsaturated porous medium where the mixture air and water coexist in the pores. Therefore, the variation of initial saturation influences the rate of the heat exchange since the heat will first evaporate the water. The highest rate of heat exchange refers to the case D where the initial saturation corresponds to lowest value (20%) and although it corresponds to lowest hot air temperature. Likewise, Fig.7 demonstrates that the fastest exchange corresponds to the lowest initial liquid saturation. The water existing inside the pores of ceramic evaporates rapidly for lower initial saturation. Moreover, the gaseous pressure inside the porous ceramic (Fig.8) shows that the highest-pressure peak corresponds to case A where highest air temperature and initial saturation are used. This behavior is explained by the fact that highest initial saturation corresponds to largest quantity of water inside the porous domain and when it is subjected to hot air (case A: 100°C) the pressure increases due to the encouraged evaporation.

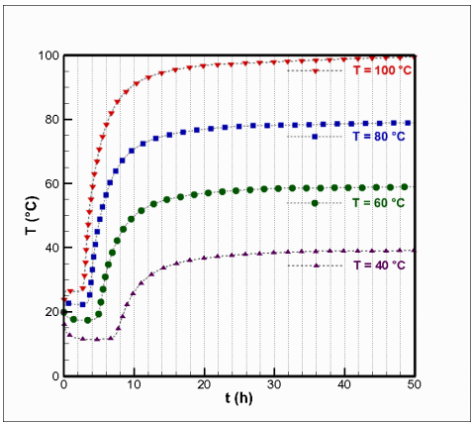

Fig. 6. Effect of hot air temperature on porous domain temperature.

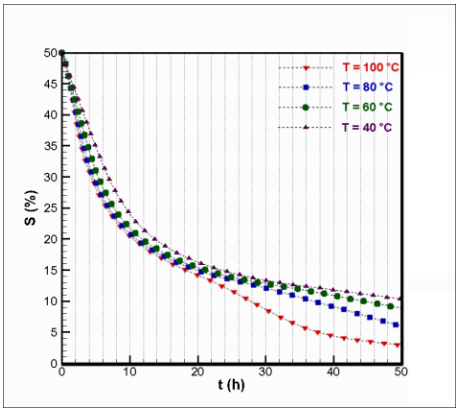

Fig. 7. Time evolution of Saturation.

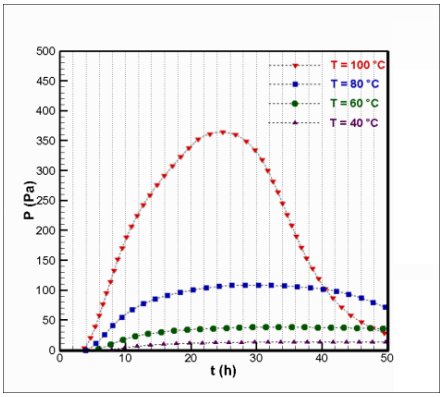

Fig. 8. Time evolution of pressure.

4.2. Effect of initial saturation of porous medium

In this part, the effect of the initial saturation of porous medium has been evaluated. Therefore, four cases have been tested (Table 5).

Table 5. Operating and initial conditions for four studied cases

	T (°C)	**S_{in}** (%)	**T_{in}** (°C)	**V** (**m/s**)	**PO** -	**CV_{amb}**	**P_{amb}** (**atm**)
Case A	100	50	20	5	0.1	0.001	1
Case B	100	40	20	5	0.1	0.001	1
Case C	100	30	20	5	0.1	0.001	1
Case D	100	20	20	5	0.1	0.001	1

Fig. 9 shows that the time evolution of the averaged porous domain temperature is highly affected by the initial saturation. Since the ceramic is considered as unsaturated porous medium where the mixture air and water coexist in the pores. Therefore, the variation of initial saturation influences the rate of the heat exchange since the heat will first evaporate the water. The highest rate of heat exchange refers to the case D where the initial saturation corresponds to lowest value (20%) and although it corresponds to lowest hot air temperature. Likewise, Fig.10 demonstrates that the fastest exchange corresponds to the lowest initial liquid saturation. The water existing inside the pores of ceramic evaporates rapidly for lower initial saturation. Moreover, the gaseous pressure inside the porous ceramic (Fig.11) shows that the highest-pressure peak corresponds to case A where highest air temperature and initial saturation are used. This behavior is explained by the fact that highest initial saturation corresponds to largest quantity of water inside the porous domain and when it is subjected to hot air (case A: 100°C) the pressure increases due to the encouraged evaporation.

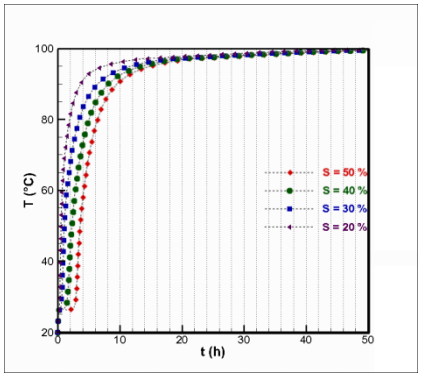

Fig. 9. Evolution of temperature.

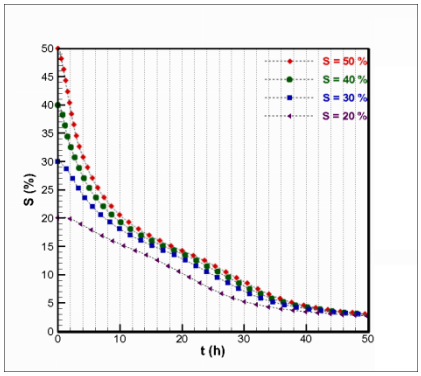

Fig. 10. Evolution of Saturation.

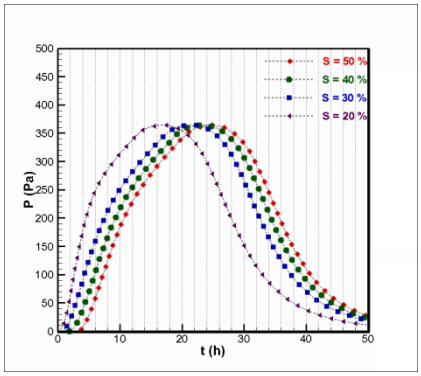

Fig. 11. Evolution of pressure.

4.3. Effect of porosity

The effect of porosity on average porous temperature, saturation and pressure evolutions are shown in Fig. 12, Fig 13, and Fig. 14 while the other porous parameters like permeability and initial saturation are fixed and for the same hot air velocity (Table 6). It can be noticed that the porous ceramic with a smaller porosity has a higher exchanging rate. Consequently, the thermal equilibrium with the hot exchanging air is attained earlier for lower porosities (Fig. 12). Moreover, ceramic with high porosities has larger evaporation rates (Fig. 13), resulting in high gaseous pressure (Fig. 14). Although, low porosity ceramic has less free area for fluid flow, resulting in increased obstruction to fluid flow when compared to high porosity ceramic, it shows slightly better heat transfer result compared to the higher porosity. This behavior may be explained by the fact that increasing porosity for the same initial liquid saturation means that the ceramic contains larger quantity of water so it will need more energy to evaporate the water existing inside the pores. Furthermore, the use of ceramic has 0.1 porosity (case E) results in time savings of 55% compared to the reference case H (0.7 porosity).

Table 6. Operating and initial conditions for four studied cases (porosity effect)

	T (°C)	**S_{in}** (%)	T_{in} (°C)	**V** (**m/s**)	**Po** -	**CV_{amb}**	**P_{amb}** (**atm**)
Case E	100	50	20	5	**0.1**	0.001	1
Case F	100	50	20	5	**0.3**	0.001	1
Case G	100	50	20	5	**0.5**	0.001	1
Case H	100	50	20	5	**0.7**	0.001	1

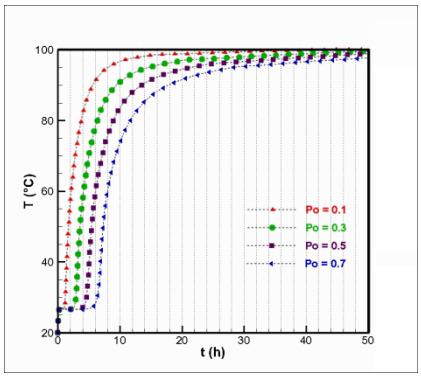

Fig. 12. Temperature evolution for different values of porosity.

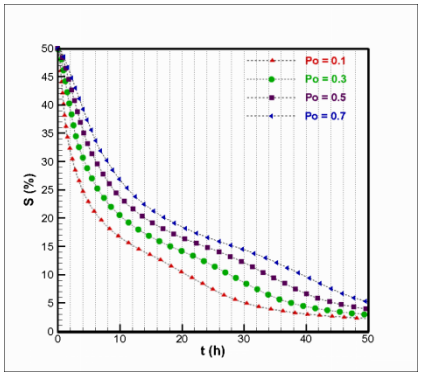

Fig. 13. Saturation evolution for different values of porosity.

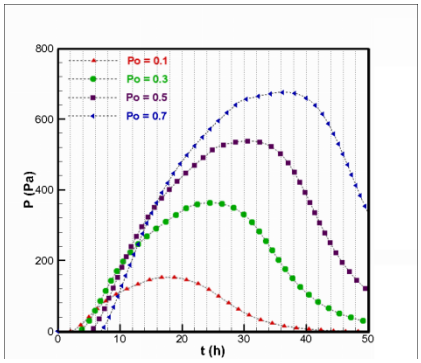

Fig. 14. Pressure evolution for different values of porosity.

Referring to Fig. 15, representing the 3D distributions of temperature, saturation and pressure inside the porous medium at 3h, since only the cavities are exchanging mass and heat within the hot circulating air, it can be seen that the heat propagates through the exchanging cavities to the whole porous ceramic domain. From liquid saturation distributions it is clear that the water migrates to the exchanging faces to evaporate on the surface. The water extraction is caused by the thermal gradient between the hot air and the porous ceramic. Once the water is completely evaporated the inner pressure becomes equal to the ambient pressure. This behavior is clearly shown by the pressure distribution inside the porous domain.

The decrease in porosity leads to higher heat exchange and faster thermal diffusion occurs in the vicinity of the exchanging cavities at earlier stages compared to higher porosities. The high porosity favorites the migration of liquid towards the exchange cavities but since the larger porosities results in larger water quantities so larger amount of heat are consumed to evaporate water before increasing the overall ceramic temperature and reaching the thermal equilibrium. This implies a faster exchange time is obtained for low porosity. Moreover, the increase of porosity implies the presence of larger water quantity inside the exchanger, which results in a higher-pressure profile.

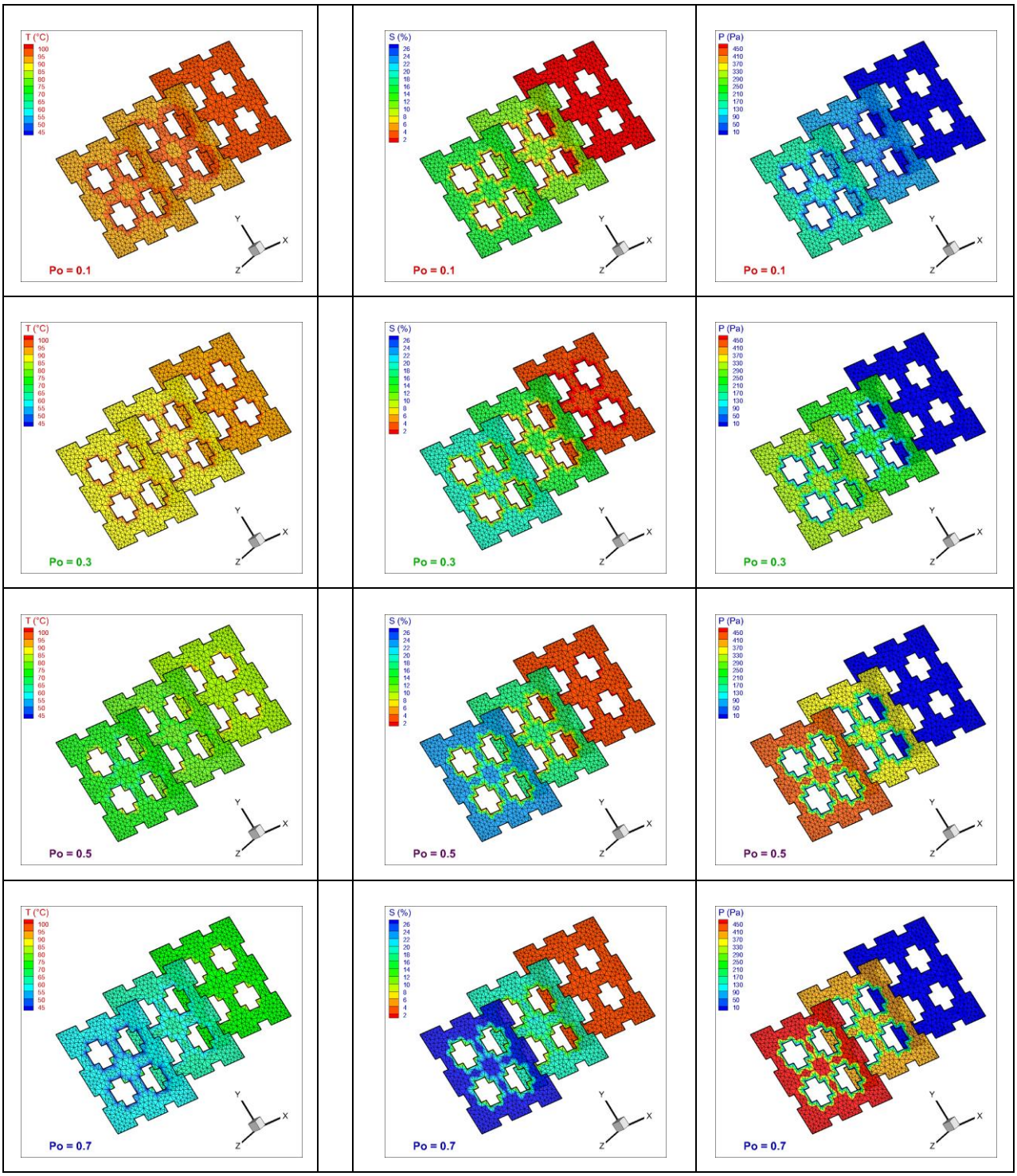

Fig. 15. 3D distributions of temperature, saturation and pressure for different porosity values after 3h.

4.4. Effect of hot air velocity

Also, we have studied the effect of hot air velocity on heat and mass transfer during porous exchanger process. Since the geometry of heat exchanger is kept the same for all the different studied cases, the variation of Reynolds number implies the variation of air velocity. For this

reason, the effect of hot air velocity has been evaluated (table 7). Consequently, the evolution of temperature, liquid saturation and gaseous pressure are presented for four velocity values (Fig. 16-18):

Table 7. Operating and initial conditions for four studied cases (porosity effect)

	T (°C)	**S_{in}** (%)	T_{in} (°C)	**V** (**m/s**)	**Po** -	**CV_{amb}**	**P_{amb}** (**atm**)
Case I	100	50	20	**5**	0.5	0.001	1
Case G	100	50	20	**10**	0.5	0.001	1
Case K	100	50	20	**20**	0.5	0.001	1
Case L	100	50	20	**30**	0.5	0.001	1

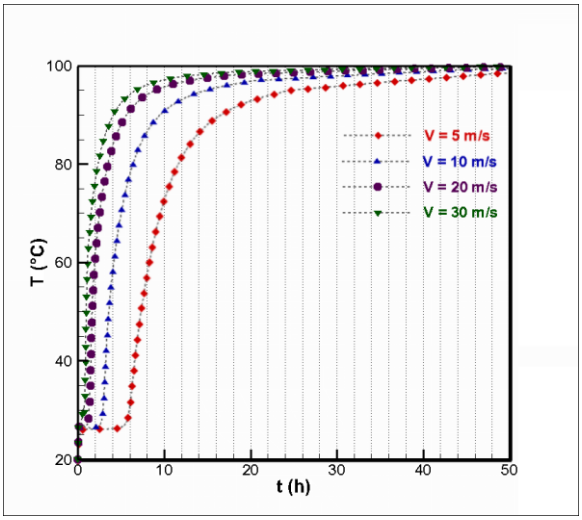

Fig. 16. Evolution of temperature for different values of velocity.

As shown in Fig.16, the fastest temperature curve corresponds to the highest value of hot air velocity. The increase in hot air velocity causes a rise in the convective heat transfer coefficient, resulting in the maximum exchanging rate for high air velocity.

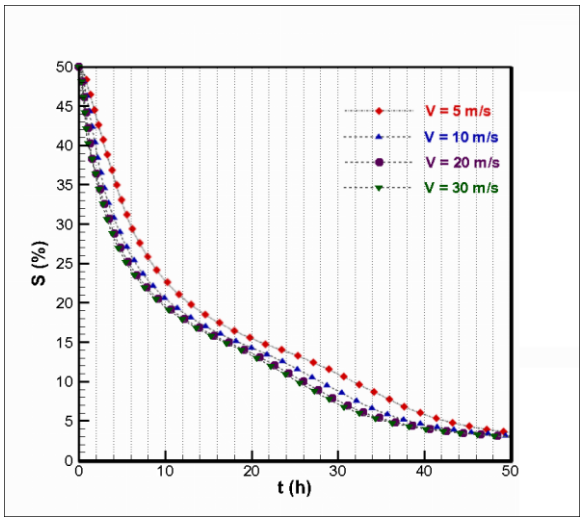

Fig. 17. Evolution of liquid saturation for different values of velocity.

Likewise, in Fig. 17 we can observe that any decrease of velocity is accompanied by a slower decrease in liquid saturation. This can be justified by the analogy between transfer mass coefficient and convective heat transfer coefficient. The latter increases with air velocity and similarly the mass transfer coefficient. As a result, higher rate of evaporation is obtained for higher velocities.

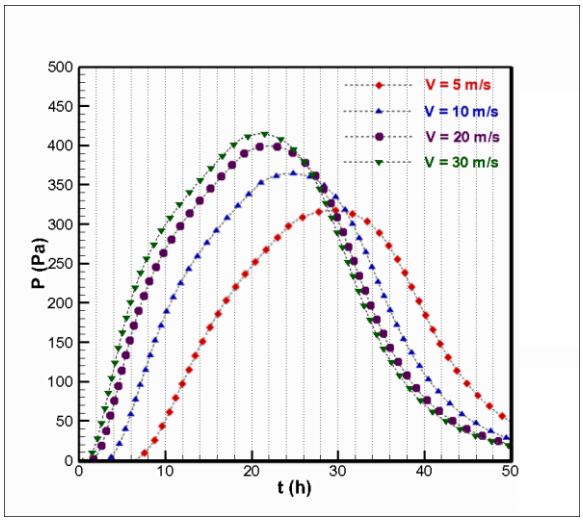

Fig. 18. Evolution of gaseous pressure for different values of velocity.

For the gaseous pressure, we note that any increase in hot air velocity results a rapid and intense pressure (Fig. 18). This phenomenon may be explained by the rise in evaporation rate produced by the increase in heat and mass transfer coefficients owing to increased air velocity. The case L corresponding to V=30m/s, leads to a time saving of 81% comparing to the case I (V=5m/s). Moreover, the results show that doubling the air velocity shortens the exchanging time by 50%, as compared to the reference case I (V=5m/s).

The slices' view to represent the distribution of temperature, liquid saturation, and gaseous pressure for different velocity values after 3h are depicted in Fig. 19. The increase of the velocity induces an intense and rapid heat exchange detected by high temperature near the exchanging cavities. Likewise, lower liquid saturation is noticed near the exchanging cavities at early stage for high air velocities. As a result, for high velocity, high pressure is seen inside the ceramic which is responsible for water extraction to the exchanging surfaces. Such behaviour can be explained by strengthening of the heat and mass transfer coefficients that lead to intense exchange and high temperature field within the porous ceramic HX.

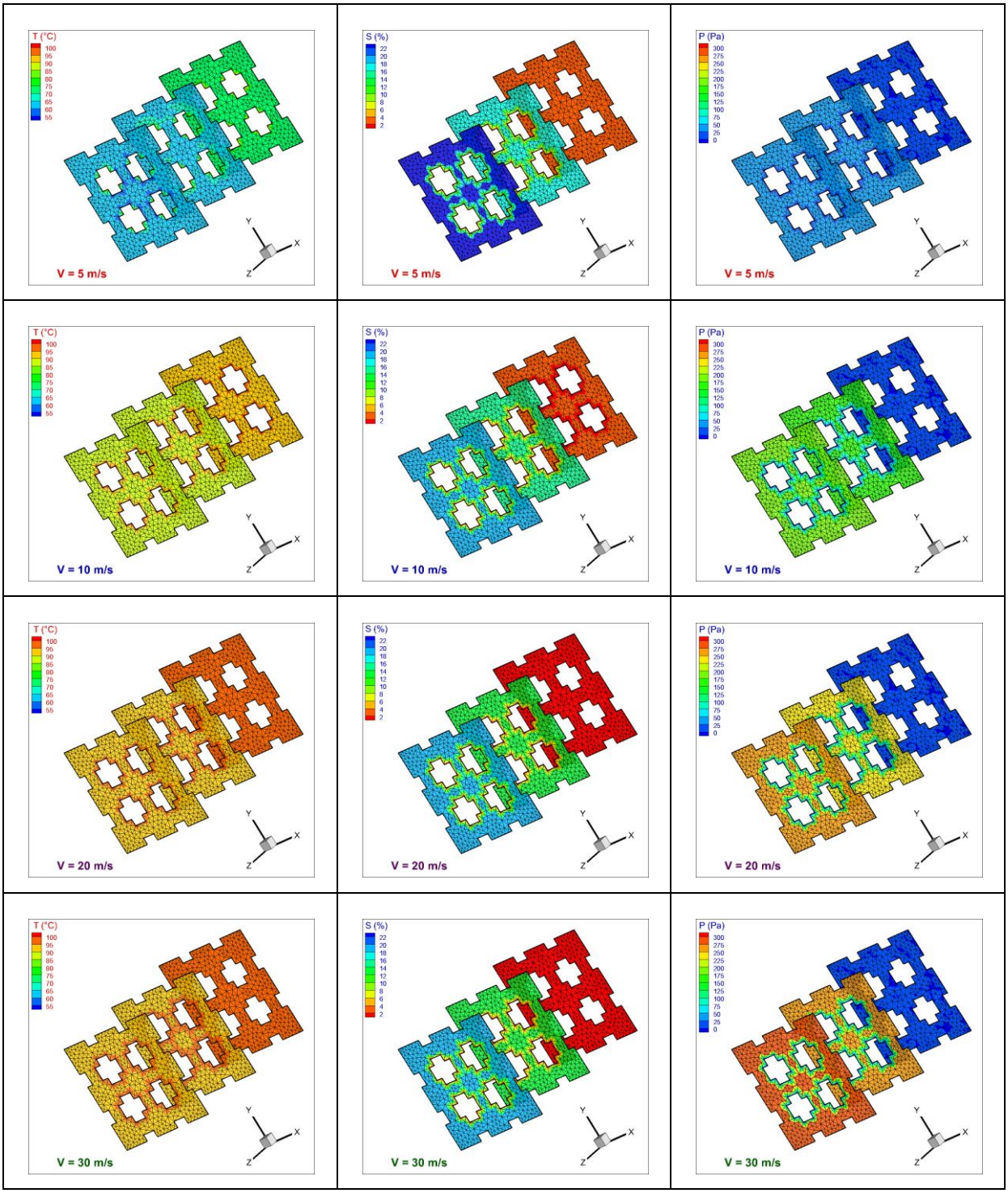

Fig. 19. 3D distributions of temperature, saturation and pressure for different air velocities after 3h

5. Conclusions

In this study, a three-dimensional numerical model was developed to investigate the effects of key parameters—temperature, liquid saturation, porosity, and hot air velocity—on heat and

mass transfer within a compact porous heat exchanger. The computational mesh was generated using the open-source mesh generator Gmsh, and a dedicated Fortran code was implemented to solve the governing equations. The model effectively captures how variations in temperature, saturation, porosity, and air velocity influence the thermal exchange performance. Based on the simulation results, the following conclusions are drawn:

- Operating conditions, particularly initial liquid saturation and hot air temperature, must be carefully selected. The heat exchange rate increases as the initial liquid saturation of the porous ceramic medium decreases.
- The heat transfer coefficient rises with increasing hot air velocity, promoting faster and more intense heat exchange. Similarly, mass transfer efficiency improves with higher air velocities.
- The porosity of the ceramic material is critical for maximizing heat transfer. For example, using a ceramic with a porosity of 0.1 reduces the exchange time by 55% compared to a reference case with 0.7 porosity.
- Increasing the air velocity to V = 30 m/s results in an 81% reduction in exchange time compared to the case with V = 5 m/s.
- Overall, doubling the air velocity effectively halves the heat exchange time relative to the reference velocity of V = 5 m/s, demonstrating the strong influence of air flow on system performance.

DATA AVAILABILITY STATEMENT

All data generated or analyzed during this study are included in this published article.

References

1. Iamsakulpanich, P., et al. (2018). Numerical simulation of porous media combustion for high temperature heat exchanger. MATEC Web of Conferences, 192

2. Alhusseny, A., et al. (2023). A POROUS MEDIA APPROACH FOR NUMERICAL OPTIMISATION OF THERMAL WHEEL. Kufa Journal of Engineering, 14(4), 56-68

3. Lochan, R., et al. (2016). Heat Transfer Improvement in Heat Exchanger using Porous Medium: a Review [Review of Heat Transfer Improvement in Heat Exchanger using Porous Medium: a Review]. International Journal of Innovative Research in Engineering & Management, 3(6), 468-470

4. Deptulski, R. C., et al. (2020). Flow and heat transfer in anisotropic active foam porous media wall. MATEC Web of Conferences, 330
5. Qader, F. F., et al. (2023). Enhancement of Double-Pipe Heat Exchanger Effectiveness by Using Porous Media and TiO2 Water. CFD Letters, 15(4), 31-42
6. Carballo, A. A., et al. (2023). Numerical and experimental study of open-cell foams for the characterization of heat exchangers. arXiv (Cornell University)
7. Carballo, A. A., et al. (2023). Numerical and experimental study of open-cell foams for the characterization of heat exchangers. International Journal of Heat and Mass Transfer, 217(15)
8. Maes, J., & Menke, H. (2022). GeoChemFoam: Direct modelling of flow and heat transfer in micro-CT images of porous media. Heat and Mass Transfer, 58(11), 1937-1947
9. Deptulski, R. C., et al. (2020). Active wall through a porous media foam type: flow and transfer characterization. MATEC Web of Conferences, 330
10. Piller, M., et al. (2014). Pore-scale simulation of laminar flow through porous media. Journal of Physics Conference Series, 501
11. Zavattoni, S. A., et al. (2021). Conceptual design and performance evaluation of an innovative high temperature ceramic heat exchanger. Journal of Physics Conference Series, 2116
12. Das, S., et al. (2016). Direct numerical simulation for flow and heat transfer through random open-cell solid foams: Development of an IBM based CFD model. Catalysis Today, 273, 140-150
13. Skibiński, J., et al. (2019). Influence of Pore Size Variation on Thermal Conductivity of Open-Porous Foams. Materials, 12
14. Haussener, S., et al. (2009). Tomography-Based Heat and Mass Transfer Characterization of Reticulate Porous Ceramics for High-Temperature Processing. Heat Transfer summer conference, San Francisco, California, USA, 33-44
15. Pullar, R. C., et al. (2019). A Review of Solar Thermochemical CO2 Splitting Using Ceria-Based Ceramics With Designed Morphologies and Microstructures. Frontiers in Chemistry, 7
16. Kozhukhov, N. N., et al. (2021). Modeling of heat transfer in an element with anisotropic porosity. Journal of Physics Conference Series, 2039
17. Zengliang, C., et al. (2024). Optimization Design and Performance Study of a Heat Exchanger for an Oil and Gas Recovery System in an Oil Depot. Energies, 17
18. Geunhyeong, L., et al. (2024). Design optimization of heat exchanger using deep reinforcement learning. International Communications in Heat and Mass Transfer, 159

19. Whitaker, S. (1977). Simulation heat, mass and momentum transfer in porous media a theory of drying. Advances in Heat Transfer, 13, 119-203
20. Dittus, F. W., & Boelter, L. M. K. (1985). Heat transfer in automobile radiators of the tubular type. Int. Comm. Heat Mass Transfer, 12, 3–22.
21. Incropera, F. P., & De Witt, D. P. (2002). Fundamentals, Heat and Mass Transfer. John Wiley & Sons, New York, USA
22. Rzig, R., Ben Khedher, N., & Ben Nasrallah, S. (2017). Three-dimensional simulation of mass and heat transfer in drying unsaturated porous medium. Heat Transfer Research, 48(11), 985-1005
23. Khedher, N. B., & Nasrallah, S. B. (2010). Three-dimensional modeling and analysis of a porous thermal energy storage system. Journal of Applied Fluid Mechanics, 3
24. Hussain, A., et al. (2006). Heat and mass transfer in tubular ceramic membranes for membrane reactors. International Journal of Heat and Mass Transfer, 49, 2239–2253